Journal of Structural Geology 32 (2010) 1576–1589

Contents lists available at ScienceDirect

Journal of Structural Geology

journal homepage: www.elsevier.com/locate/jsg

Internal structure, fault rocks, and inferences regarding deformation, fluid flow, and mineralization in the seismogenic Stillwater normal fault, Dixie Valley, Nevada

Jonathan Saul Caine [a,*], Ronald L. Bruhn [b], Craig B. Forster [b]

[a] U.S. Geological Survey, P.O. Box 25046, MS 964, Denver, CO 80225, USA
[b] Department of Geology and Geophysics, University of Utah, 115 South 1460 East, Salt Lake City, UT 84112, USA

ARTICLE INFO

Article history:
Received 15 January 2009
Received in revised form
28 January 2010
Accepted 9 March 2010
Available online 17 March 2010

This work is dedicated to the memory of Craig B. Forster who died in a tragic accident on December 28, 2008. It is a reflection of his exceptional enthusiasm and dedication to bringing students and colleagues together in the pursuit of collaborative scientific research.

Keywords:
Fault zone
Seismicity
Fluid flow
Hydrothermal
Breccia textures
Silicification

ABSTRACT

Outcrop mapping and fault-rock characterization of the Stillwater normal fault zone in Dixie Valley, Nevada are used to document and interpret ancient hydrothermal fluid flow and its possible relationship to seismic deformation. The fault zone is composed of distinct structural and hydrogeological components. Previous work on the fault rocks is extended to the map scale where a distinctive fault core shows a spectrum of different fault-related breccias. These include predominantly clast-supported breccias with angular clasts that are cut by zones containing breccias with rounded clasts that are also clast supported. These are further cut by breccias that are predominantly matrix supported with angular and rounded clasts. The fault-core breccias are surrounded by a heterogeneously fractured damage zone. Breccias are bounded between major, silicified slip surfaces, forming large pod-like structures, systematically oriented with long axes parallel to slip. Matrix-supported breccias have multiply brecciated, angular and rounded clasts revealing episodic deformation and fluid flow. These breccias have a quartz-rich matrix with microcrystalline anhedral, equant, and pervasively conformable mosaic texture. The breccia pods are interpreted to have formed by decompression boiling and rapid precipitation of hydrothermal fluids whose flow was induced by coseismic, hybrid dilatant-shear deformation and hydraulic connection to a geothermal reservoir. The addition of hydrothermal silica cement localized in the core at the map scale causes fault-zone widening, local sealing, and mechanical heterogeneities that impact the evolution of the fault zone throughout the seismic cycle.

Published by Elsevier Ltd.

1. Introduction

The presence and flow of fluids in the upper crust has a major impact on the mechanics of faulting (Hubbert and Rubey, 1959; Nur and Booker, 1972; Sibson, 1977, 1981, 1990, 1996; Power and Tullis, 1989; Bruhn et al., 1990, 1994; Parry and Bruhn, 1990; Scholz, 2002; Chester et al., 1993; Rice, 1992; Byerlee, 1993; Keller and Loaiciga, 1993; Evans and Chester, 1995; Caine et al., 1996; Miller et al., 1996; Seront et al., 1998; Tanaka et al., 2001; Wibberley, 2002;Faulkner et al., 2006; Lockner et al., 2009). Fluid flow and its interactions with heterogeneous permeability structures in a fault zone can control the magnitude of local principal stresses (Nemcok et al., 2002). This, in turn, affects local fluid-pressure gradients, mechanical failure, propagation of pressure transients, fluid infiltration into and out of a fault zone via fault-valve mechanisms (e.g., Sibson, 1992), and fault-zone sealing and healing (e.g., Faulkner et al., 2008). Fluid flow in fault zones can control the location, emplacement, and evolution of economic mineral deposits and geothermal systems (e.g., Newhouse, 1942; Cox et al., 2001; Sibson, 2001; Micklethwaite, 2009), and may also impact the locations and magnitudes of foreshock, earthquake and aftershock distributions (Miller et al., 2004). Yet fault zones are heterogeneous geological and hydrological structures that commonly are not well exposed. Even in well-exposed fault zones direct links between internal structure, fault rocks, and mineral assemblages that uniquely indicate a seismogenic origin are uncommon (cf. Sibson, 1986b; Cowan, 1999; Ujiie et al., 2007; Woodcock et al., 2007; Smith et al., 2008). Thus, the study of exposed, seismogenic fault zones that may record fluid flow-related processes associated with earthquakes remains important for understanding the mechanics of faulting.

* Corresponding author.
E-mail address: jscaine@usgs.gov (J.S. Caine).

0191-8141/$ – see front matter Published by Elsevier Ltd.
doi:10.1016/j.jsg.2010.03.004

Fault zones are commonly composed of distinct, three-dimensional, mappable components that include a fault core and damage zone within relatively undeformed protolith (Chester and Logan, 1986; Smith et al., 1990; Forster et al., 1991; Caine et al., 1996). Most of the strain is accommodated in a fault core indicated by rocks such as fault-related breccias and clay-rich gouge. Fault zones can also have multiple core zones interspersed with pods of heterogeneously deformed host rock (cf. Faulkner et al., 2006). A damage zone is the mappable network of subsidiary structures that surrounds a fault core or fault-core zone and is related to the nucleation, evolution, and growth of the fault zone (Chester and Logan, 1986; Scholz, 2002; Caine et al., 1996; Knipe et al., 1998). Damage-zone fracture networks commonly have orientations mechanically related to the master fault and are of higher intensity than found in the protolith (e.g., Caine and Forster, 1999). The fault core and damage zone are surrounded by the protolith where fault-related structures are generally absent.

The bulk permeability structure and strength of a fault zone are controlled by preexisting and newly developed structures, the regional and local stress state, fault-zone geometry, and changes in lithology resulting from the coupling of mechanical, thermal, fluid flow, and reactive geochemical processes. For example, the creation of new hydraulically contrasting lithologies and structures, such as clay-rich cataclasites and complex fracture networks, has been documented to result from as well as impact fluid flow in diverse brittle fault-zone settings (Sibson, 1986a; Chester and Logan, 1986; Scholz, 2002; Bruhn et al., 1994; Antonellini and Aydin, 1994; Goddard and Evans, 1995; Caine et al., 1996; Faulkner et al., 2006). These fault-related physical attributes in the upper crust create hydraulic and mechanical heterogeneity and anisotropy that have a significant impact on rupture and the arrest of failure (Parry et al., 1991; Byerlee, 1993; Miller et al., 1996; Seront et al., 1998) as well as growth and widening of a fault zone.

Previous theoretical research in earthquake mechanics has focused on the role of fluid circulation and hydrothermal alteration associated with faulting processes (Sibson, 1981; Bruhn et al., 1994; Parry et al., 1991; Rice, 1992; Byerlee, 1993; Scholz, 2002; Unsworth et al., 1997). Although there have been studies of exhumed and well-exposed seismogenic fault zones (e.g., Hancock and Barka, 1987; Ghisetti et al., 2001), details regarding the physical pathways along which fluid flow occurs, and the characteristics of structures and rock types that result from coupled deformation and fluid flow remain sparsely documented.

This paper describes field observations from the Mirrors locality of the Stillwater Fault Zone (SFZ) in Dixie Valley, Nevada (Fig. 1). This is an area of geological interest due to exposures of exhumed portions of the footwall of this normal fault with a record of historic earthquakes and surface ruptures associated with the fault. There are also epithermal gold deposits, and a productive geothermal reservoir hydraulically connected to the fault zone. Outcrop mapping, hand-sample and thin-section fault-rock studies are used to extend previous work and (1) document the internal structure and geometry of part of the fault zone, (2) infer the paleo-permeability structure, (3) document the textural attributes, composition, and spatial and temporal distribution of fault rocks, and (4) infer deformation-related fluid flow processes associated with seismicity and growth of the fault zone.

2. Geologic setting and previous work

The SFZ is historically active and capable of generating magnitude (M) > 6 earthquakes. Ground surface rupture associated with the 1954 $M = 6.8$ earthquake was 30–40 km long (Caskey et al., 1996). The SFZ, also called the Dixie Valley Fault, is the eastern range-bounding fault between the Stillwater Mountains and Dixie Valley graben (Fig. 1). Fault segments that range from several kilometers to a few tens of kilometers in length form the SFZ. The SFZ is one segment in a 300 km long belt of normal and normal-oblique slip faults (Wallace and Whitney, 1984; Caskey et al., 1996). The Stillwater Range is composed of Mesozoic metasedimentary, plutonic, and volcanic rocks. Igneous rocks include the Jurassic gabbroic Humboldt igneous complex, Cretaceous granites, a multiphase Oligocene granite–granodiorite–quartz monzonite complex, and various extrusive rocks of Oligocene and Miocene age (Page, 1965; Speed and Armstrong, 1971; Wilden and Speed, 1974; Speed, 1976).

The SFZ has been seismically active since Oligocene to early Miocene times (Parry et al., 1991; Bruhn et al., 1994; Caskey et al., 1996; Seront et al., 1998). The Holocene fault scarps that cut the basin fill along the eastern base of the Stillwater Range are ground surface ruptures probably formed during major earthquakes within

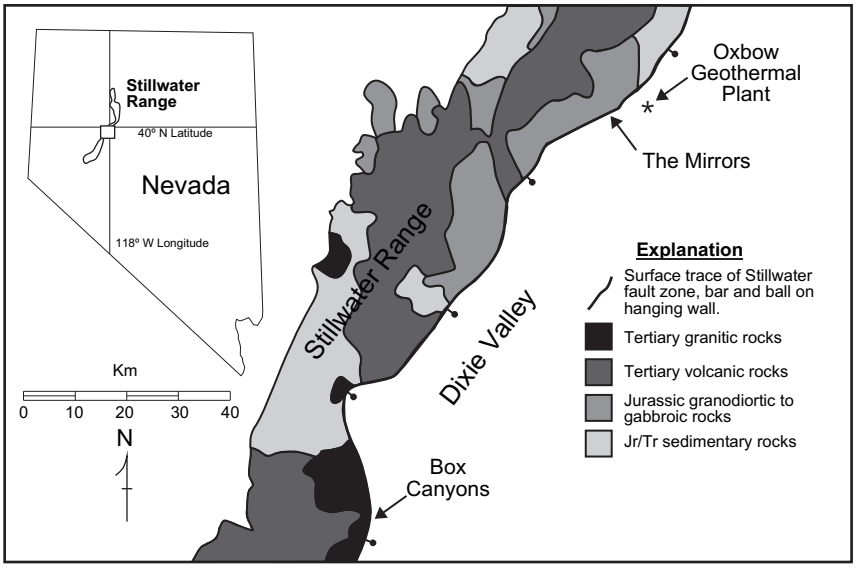

Fig. 1. Location map for the Stillwater Fault Zone in Dixie Valley, Nevada showing the primary study area of the Mirrors Locality. Modified from Parry and Bruhn (1990).

the last 12,000 years (Wallace and Whitney, 1984; Caskey et al., 1996). The eastern slope of the Stillwater Range is the exhumed footwall of the fault zone. An along-strike differential surface-uplift history of the Stillwater Range is suggested by rocks exhumed from a minimum depth of 6 km (Parry et al., 1991) in the southern part of the range and as little as 2 km at temperatures less than 270 °C in the central part of the range (Power and Tullis, 1989).

The rocks exposed along the SFZ and at the Mirrors locality in the central part of the Stillwater Range have undergone varying degrees of hydrothermal alteration that includes the following mineral assemblages and paragenetic sequence: biotite + K-feldspar, chlorite + sphene + epidote + magnetite; mixed-layer chlorite–smectite + smectite + goethite; quartz + illite + calcite + ferroan dolomite + calcite + barite; quartz + kaolinite; and quartz + calcite (Parry et al., 1991; Lutz et al., 1997). The assemblages in this paragenetic sequence were interpreted to preserve a record of exhumation, with the earlier assemblages also representing deeper crustal conditions. Power and Tullis (1989) present a detailed analysis of slip surfaces at the Mirrors and make estimates of deformation temperatures based on the thermodynamic stability of the quartz + kaolinite mineral assemblage in distinctive fault-related breccias and the tectonostratigraphic position of this locality with respect to overlying volcanic rocks. They observed crystallographic preferred orientation of quartz c-axes in samples of the slickensided surfaces and their preferred interpretation of this alignment involves pressure solution and growth/dissolution rate anisotropy during continuous, low temperature, low strain-rate deformation. Additionally, Power and Tullis (1989) interpreted multiple generations of fault-related brecciation and thus interpreted alternating periods of continuous deformation during the interseismic phases of the earthquake cycle followed by discontinuous deformation during coseismic phases of the earthquake cycle.

Hydrothermal alteration in the Oligocene granitic complex along the base of the Stillwater Range reflects the interplay of faulting, fluid circulation, and exhumation associated with the SFZ (Parry et al., 1991; Lutz et al., 1997). At some localities this alteration may reflect fault-related fluid interactions with an ancient, and presently producing, geothermal reservoir as well as a number of surficial expressions of the geothermal system such as hot springs, sinter mounds, and fumaroles (e.g., Lutz et al., 2002). Barton et al. (1997) and Hickman et al. (1997, 1998, 2000) studied borehole log and *in situ* stress data near the Oxbow geothermal plant, several kilometers northeast of the Mirrors locality (Fig. 1). They found that the hydraulically conductive fractures in the geothermal reservoir were also critically stressed for shear failure in the regional stress field. Finally, structurally favorable sites and fault-related fracture networks also create loci for hydrothermal fluid flow that produced economic epithermal gold deposits (e.g., Vikre, 1994).

3. The Mirrors map area exposure, overview, and methods

Each fault-zone component is well exposed in the bedrock at the Mirrors locality (Figs. 2–4). This footwall remnant of the SFZ extends approximately 250 m vertically upward from the base of the Stillwater Range. Although the hanging wall is composed of Quaternary basin fill in depositional contact with the crystalline footwall and no recent ground surface rupturing fault scarps were observed directly against it, we have mapped this as a fault contact to portray the crystalline fault rocks in juxtaposition with the fill (Figs. 2 and 3). It is likely that recent fault scarps exist in the fill but mapping these was beyond the scope of our work. There are no exposures of the crystalline hanging wall at the Mirrors. The exposed fault core is complex but ranges in thickness from ~1 to 5 m. However, partial erosion of the core makes it difficult to estimate the *in situ* thickness or geometry of the entire fault core. Although previously mapped as hornblende gabbros and anorthosites of the Jurassic Humboldt igneous complex (Speed, 1976), the protolith at the Mirrors locality is a fine to medium-grained granodiorite with chloritization of biotite and hornblende in the protolith and variable chloritic to argillic to silicic alteration in the damage zone.

Semiquantitative X-ray diffraction (XRD) patterns were obtained from representative, whole-rock samples of each fault zone component (Table 1). The samples were X-rayed with a quartz standard and Cu-Kα radiation from 5° to 90° two-theta. Spectra

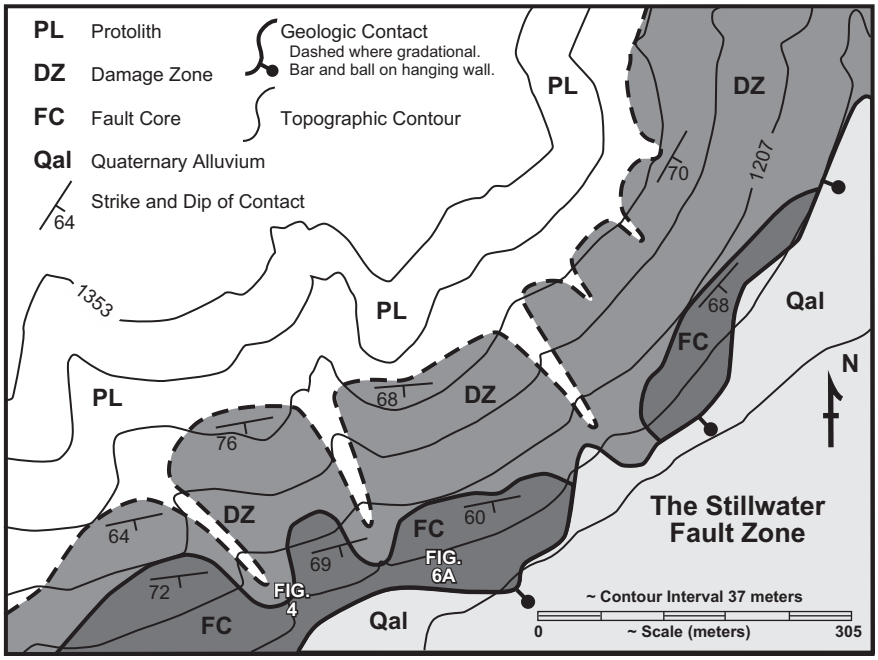

Fig. 2. Simplified geologic map of the Stillwater Fault Zone at the Mirrors Locality. Note that the protolith/damage-zone contact is gradational (dashed line) and the damage-zone/fault-core contact is abrupt (solid line). The approximate locations of Figs. 4 and 6A are shown for reference.

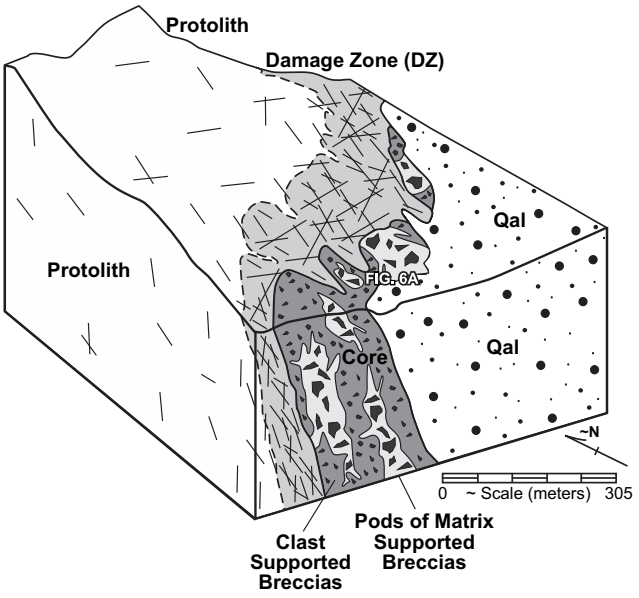

Fig. 3. Schematic block diagram showing breccia pods, clast and matrix-supported breccias in the fault core. Note the abrupt contact between the fault core and damage zone and the gradational contact between the damage zone and the protolith. The approximate location of Fig. 6A is shown for reference. Qal = Quaternary alluvium.

were manually matched to library peak intensity data for individual mineral determination and the estimated error for each reported mineral is ±10 weight percent.

The contacts between, and physical properties of, the fault core, damage zone, and protolith were mapped using standard tape and compass techniques using a 1:24,000 topographic base map blown up to a scale of approximately 1:6,000 (Figs. 2 and 3). Detailed fracture and vein data (e.g., orientation, intensity, and failure mode interpretation, i.e., shear or extension fracture) were also collected and used to help define each architectural component. Fracture data were collected using standard scanline and grid counting methods (e.g., Priest, 1993) in three perpendicular directions related to strike, dip, and slip direction of the fault zone (e.g., Seront et al., 1998; Caine and Forster, 1999) at a variety of representative outcrops. Data were integrated across a number of scales of observation with centimeter-scale petrographic analyses, meter-scale outcrop mapping, and at tens to hundreds of meters-scales using low-elevation aerial photographs.

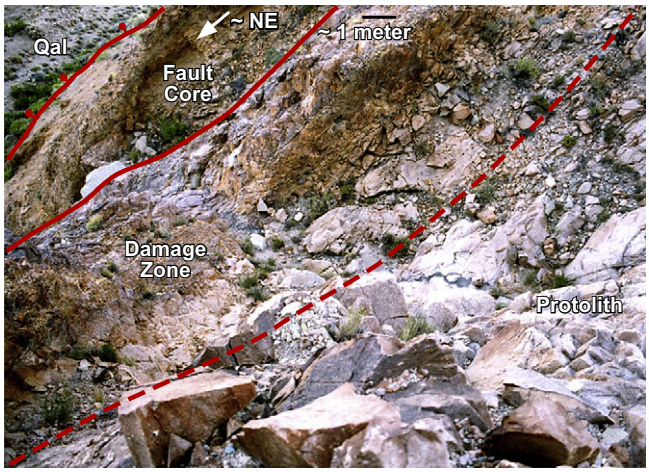

Fig. 4. Photograph of the footwall, fault-zone components and contacts. Diagonally from left to right in the photograph are Quaternary alluvium, the brecciated and silicified fault core, the highly fractured damage zone, and the gradational contact between the damage zone and the relatively less fractured protolith.

4. Fault zone structure and fault rocks

4.1. Fault zone orientation, component contact relationships, and mineralogy

The SFZ strikes northeast to east-northeast and dips from 32° to 70° southeast (Figs. 1–5). The broad range in orientation of major slip surfaces shown in Fig. 5 reflects significant map to outcrop-scale variation in the topography of multiple slip surfaces (cf. Power and Tullis, 1989; Sagy et al., 2007). Slickenlines indicate that the fault is dominantly normal dip–slip with minor components of left and right lateral strike–slip (Fig. 5).

Figs. 2 and 3 show that the fault core and damage zone are tabular to curvitabular bodies. The contact between the fault core and damage zone is marked by an abrupt transition between the cataclastic rocks and distinct breccia bodies of the core and highly fractured and veined granodiorite of the damage zone (Figs. 2–4). Portions of this contact are marked by a single curviplanar, polished and striated slip surface, whereas at other locations the fault rocks at the contact are breccias. Some polished slip surfaces are on the order of 100 m^2, exposed over a strike distance of about 100 m (Fig. 6A). Additionally, distinct and overlapping slip surface sheets of polished and striated quartz within the core show different lineation directions. In some locations several, anastomosing primary slip surfaces exist at the contact and it is unclear if only one or all of these were active during deformation. The fault-core and damage-zone contact is both a structural and a lithologic contact, as the fault-core rocks are highly silicified and the damage-zone rocks generally are not. In contrast to the distinct fault-core/damage-zone contact, the contact between the damage zone and protolith is gradational and marked by decreasing fracture intensity, silicification, and argillic alteration (Figs. 2–4).

Whole-rock XRD analysis of representative samples from each fault-zone component shows spatially systematic changes in composition from the fault core to the protolith at the map to outcrop scale. Quartz is the dominant mineral in the fault core whereas plagioclase feldspar is dominant in the damage zone and protolith (Table 1). Kaolinite, carbonates, barite, hematite, chlorite, biotite, and titanium oxides are also present in the fault core and damage zone. The damage zone shows mineralogical evidence of argillic alteration compared with the protolith.

4.2. Protolith and damage-zone fracture networks

Several macroscopic fracture types were interpreted from the orientations and morphology of distinctive fracture sets relative to the average orientation of the master fault zone, assuming an Andersonian stress regime typical for normal dip–slip faults (Fig. 5; cf. Caine and Forster, 1999). Fractures that strike subparallel to the fault zone but are subvertical and planar are interpreted to be extension fractures. Curviplanar fractures oriented parallel to the fault zone that have normal dip–slip slickenlines, and (or) minor normal offsets and those that strike parallel to the fault zone but have antithetic dips, are interpreted to be shear fractures. A set of subhorizontal fractures are termed step fractures as they result in 'stepped' shaped outcrops. They are generally rough but planar to curviplanar, and are oriented at high angles to the average orientation of the master fault zone. Step fractures have an uncertain origin but may be similar to linking fractures and small faults found in compound fault zones of the Sierra Nevada of central California

Table 1
Mirrors locality X-ray diffraction data averaged for each fault zone component. Major rock forming mineral concentrations reported in weight percent, ±10 percent error. Feldspars are predominantly plagioclase and accessory minerals include chlorite, biotite, and hornblende.

Sample type (n = number of samples)	Quartz	Plagioclase + K-feldspar	Kaolinite	Carbonate	FE and TI oxides	Amorphous or accessory
Fault-core rocks						
Pink slip surface/rounded clast breccia ($n = 1$)	88	0	3	1	0	8
Clast-supported breccias ($n = 3$)	63	0	25	4	5	3
Matrix-supported breccia whole rock ($n = 3$)	79	0	10	3	3	5
Matrix supported breccia matrix only ($n = 1$)	74	0	22	2	0	2
Damage zone ($n = 4$)	24	45	9	15	5	2
Protolith ($n = 6$)	10	71	6	2	3	6

(Martel, 1990). Mixed-mode fracturing is suggested locally by the presence of horsetail-like or feather-like splay fractures (Fig. 6, cf. Micklethwaite, 2009). There are three sets of fractures that appear to have no systematic orientation with the master fault zone but cross all but the shear fracture sets and thus are termed cross fractures (Fig. 5). They are typically steeply to moderately dipping, are often smooth walled, and planar. Interestingly, the critically stressed and hydraulically conductive fractures associated with the geothermal reservoir observed by Barton et al. (1997) and Hickman et al. (1997) have reasonably similar orientations to two of the cross fracture sets and to the silicified slip surfaces found in the exhumed core of the SFZ (Fig. 5).

Macroscopic cross fractures are primarily found in the protolith but are also found in the damage zone (Fig. 5). The median fracture intensity inclusive of all fracture types observed from 11 different locations in the protolith is 16 fractures per meter with a minimum of 10 and maximum of 25 per meter. Microfracturing is not abundant in the protolith (Fig. 6). Because cross fractures are generally

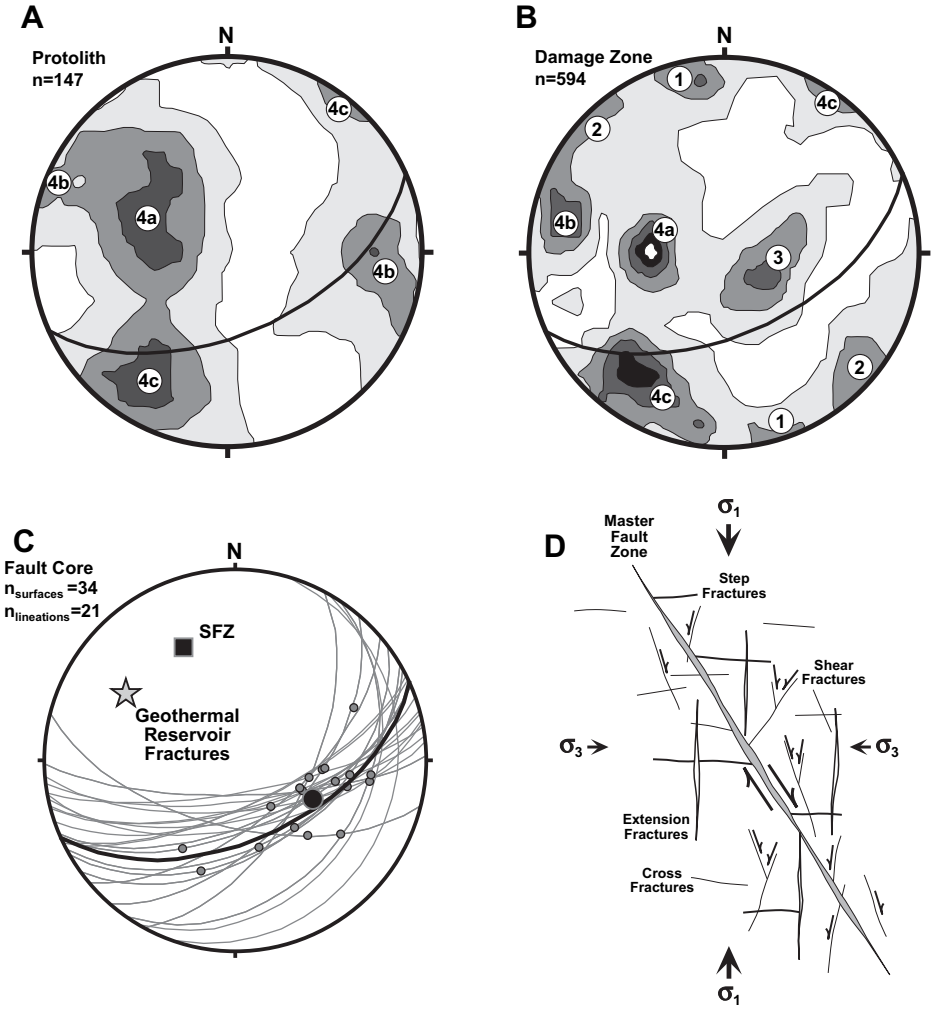

Fig. 5. Lower hemisphere, equal area projections showing orientations of structures in each fault-zone component at the Mirrors locality (A and B, Kamb contoured poles to fractures, contour interval = 2.0 sigma with the mean SFZ great circle shown in black, modified from Caine and Forster, 1999; C, great circles and slip lineations). A) Data from protolith only. B) Data from damage zone only. In A and B, fractures broken into sets from raw data are assigned to a mode of formation based on interpretation of mechanical compatibility with an Andersonian model of a normal fault. Relative to the master fault zone the following sets are defined: 1 = extension; 2 = shear; 3 = step; 4a, 4b, and 4c = cross fractures. C) Gray great circles are slip surfaces and small gray dots are the corresponding slickenlines. The black great circle and large black dot show the mean slip surface and slickenline orientations and the large black square is the pole to the mean SFZ slip surface. The gray star shows the approximate mean pole to hydraulically conductive and critically stressed fractures derived from borehole logging in the Dixie Valley geothermal reservoir within several kilometers of the Mirrors locality (from Barton et al., 1997). D) Schematic, field-based cross-section of the traces of idealized fracture sets associated with an Andersonian normal fault (modified from Caine and Forster, 1999).

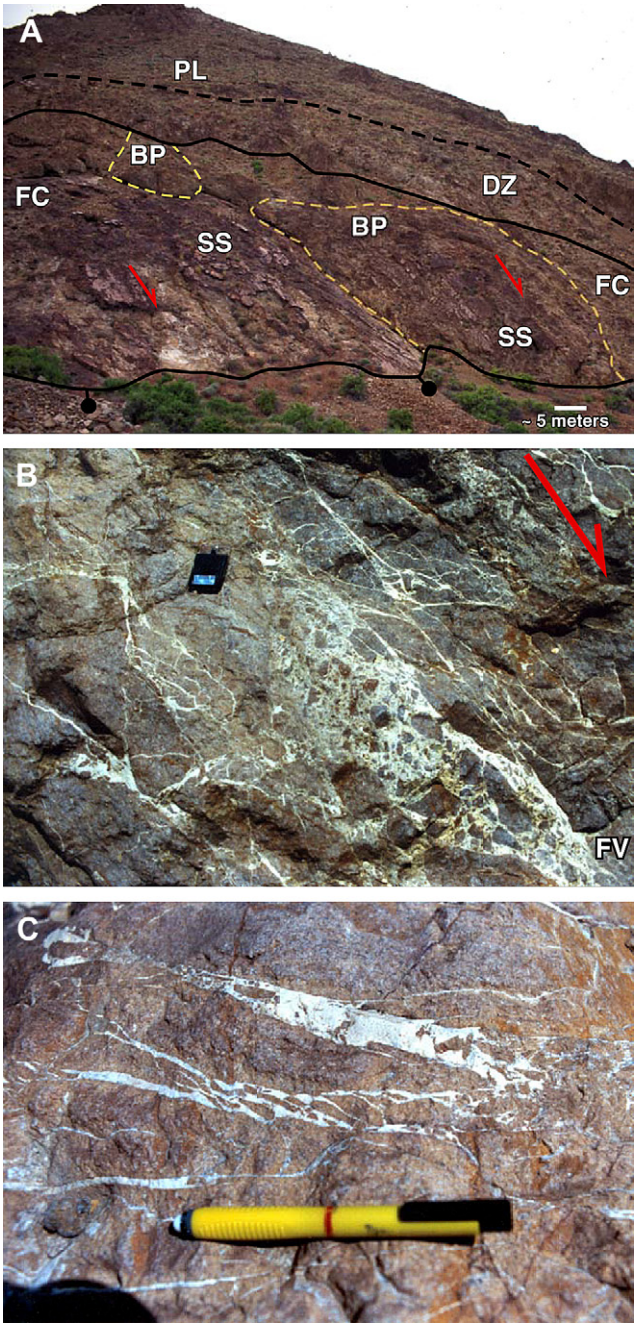

Fig. 6. A) Exposure of the main 'Mirrors' slip surfaces (SS) and large breccias pods (BP) outlined in dashed yellow. Approximate contacts between Quaternary alluvium (Qal), fault core (FC), damage zone (DZ), and protolith (PL) are shown with black lines. The large corrugated pod is composed of all breccia types, bounded by polished and striated curviplanar slip surfaces, and is elongated parallel to the average slip vector indicated by the red arrows. B) Outcrop photograph of a small (compass for scale) breccia pod with matrix-supported breccias. The long axis of the pod is subparallel to the average orientation of the master fault zone shown by the red arrow. A possible feeder vein (FV) connected to a network of very long and wide veins can be seen at the bottom central portion of the pod. C) Breccia pod veins with jigsaw puzzle breccia. Note the en échelon clasts and closing taper of the veins away from a larger breccia pod to the right of the photograph. Each photograph is a northward to northwesterward-looking view along the strike of the Stillwater Fault Zone.

cut by fault-related shear fractures, the cross fractures may have formed prior to faulting. Additionally, some cross fractures are filled with a distinctive beige quartz + kaolinite mineral assemblage that emanates from the fault core, through the damage zone and into the protolith suggesting they were possibly hydraulically conductive during faulting. Extension, shear, and step fractures do not generally occur in the protolith, suggesting that they are mechanically related to faulting as their presence is largely restricted to the damage zone (Fig. 5).

The damage zone consists of intensely fractured and veined granodiorite (Figs. 2–7). The median fracture intensity inclusive of all fracture types observed from 16 localities in the damage zone is 50 fractures per meter with a minimum of 32 and maximum of 99 per meter. Although no suitable outcrops were found where macroscopic fracture intensity changes could be continuously measured from the damage zone into the protolith, the change did not appear to be systematic from one location to another where partial observation could be made. Alteration and microfracture intensity also increase toward the fault core and silicification in the damage zone is generally restricted to veins (Fig. 7; Table 1). Damage-zone veins at all sites are filled with the same quartz + kaolinite mineral assemblage found in the fault core and many commonly have angular fragments of wall rock suspended in the matrix (Fig. 7). The veins range in width, perpendicular to their walls, from a few millimeters up to about 10 cm and have trace lengths of just under a meter up to nearly 10 m. They occur at intensities of approximately 1 vein per meter to stockworks with many tens of veins per meter. Veins are planar to curviplanar but when they occur as stockworks they can have quite irregular and jagged shapes.

4.3. Fault rocks

A representative sample from the fault core is described from hand-sample to thin-section scales (Figs. 8 and 9). This sample contains a major silicified slip surface similar to those found bounding some of the breccia pods as well as the range of different types of fault-related breccias with important cross-cutting relationships representative of the Mirrors locality. Sections cut parallel and perpendicular to slip were cut to document variations in textures, microstructures, and fault-rock compositions.

The fault core at the Mirrors locality comprises several structurally and texturally distinct fault-rock types described using elements of classifications by Sibson (1977, 1986a), Sillitoe (1985), Jébrak (1997), and Mort and Woodcock (2008) including: breccias with rounded clasts; clast-supported breccias with highly angular and interlocking clasts; matrix-supported breccias with angular clasts that could be pieced back together if the matrix was removed; breccias with open spaces between the clasts; and fault gouge described in detail below.

4.3.1. Breccias with rounded clasts

Breccias with rounded clasts are predominantly matrix supported but are also locally clast supported. They are poorly sorted with respect to size, composed of well-rounded clasts and subangular clasts, and are typically associated with cross-cutting slip surfaces. These textures are observed in the fault rocks at both the hand-sample and thin-section scales (Figs. 8 and 9). The uppermost millimeter of the hand sample shown in Fig. 8 is a polished and striated, silicified slip surface representative of those described above. In the first centimeter of the sample, from the slip surface toward the base of the polished face (Figs. 8 and 9), the sample exhibits an ultra-fine-grained, highly indurated, white–pink colored breccia matrix. Most of the clasts in this matrix show distinct clasts within clasts textures. This part of the sample is nearly identical to samples studied by Power and Tullis (1989).

In thin section, quartz is the primary mineral with minor amounts of kaolinite within about a centimeter of the slip surface (Fig. 9A and D). In Fig. 9D the section is oriented perpendicular to the strike of the fault and parallel to the slip direction. The silicified hanging wall material shows crystallographic preferred orientation

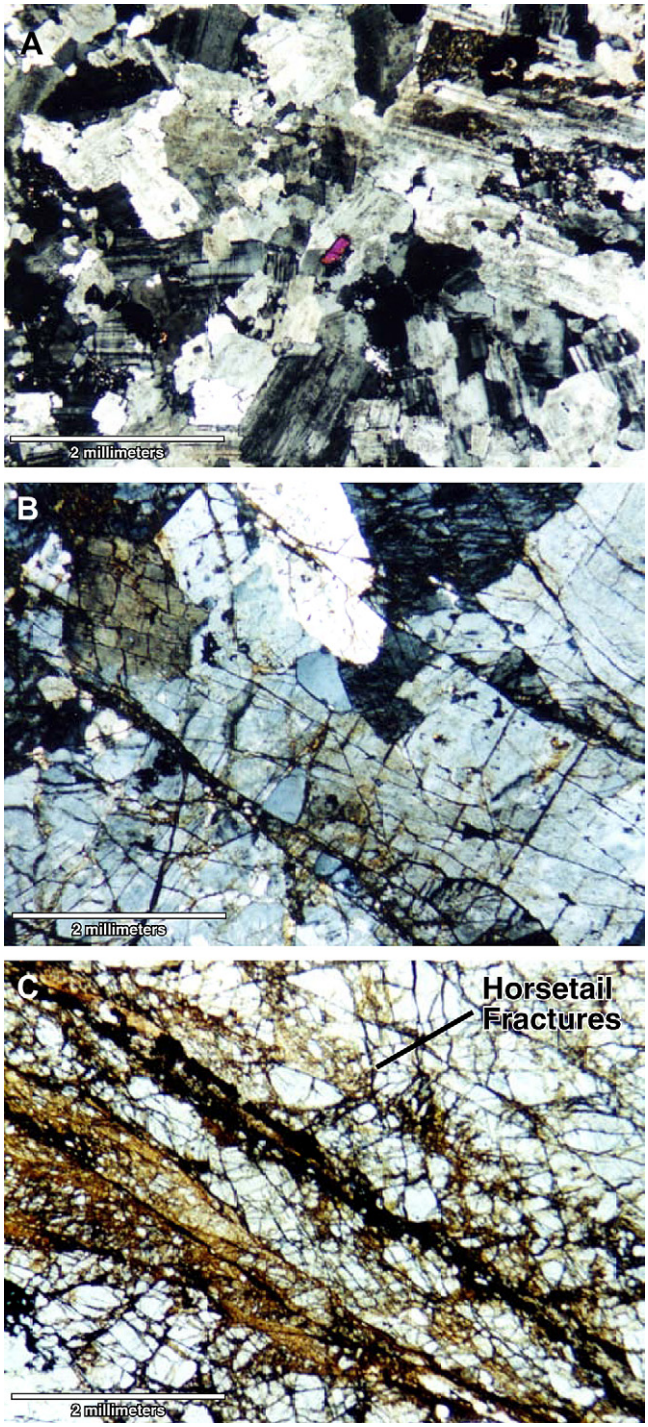

Fig. 7. Photomicrographs of representative rock samples from the protolith and damage zone. A) Polarized light image of protolith granodiorite. Equigranular quartz + plagioclase + potassium feldspar + biotite, which is altered to chlorite. Note the absence of microfracturing. B) Polarized light image of damage-zone microfractures in granodiorite ~10 m from the fault core. C) Polarized light image of damage-zone granodiorite ~5 m from the fault core shows extensive microfracturing, horsetail fractures, and silicified veins with cataclastic particles.

Fig. 8. A) Photograph of a polished hand-sample from the fault core. The top of the sample is a slip surface and the polished face is parallel to the slip direction. The three major breccia types are exhibited. Note that the breccia with rounded clasts grades into the clast-supported breccia. In contrast, the contact between the clast-supported breccia and the matrix-supported breccia is relatively abrupt indicating the cross-cutting of the former by the latter. B) Example of breccia with vuggy open space. Each iron oxide stained clast is coated with a rind of carbonate with euhedral crystals. Note the 10× hand lens for scale.

(CPO) of quartz, indicated by linear domains of common extinction in synthetic and antithetic microfaults as described in detail by Power and Tullis (1989) and is typical of breccia pod bounding slip surfaces. Scanning electron microscopy shows quartz occurs as microcrystalline prisms on the order of 10 μm long with approximate alignment with the synthetic microfaults (Fig. 9E). Quartz with CPO also occurs as micron-scale coatings surrounding many of the clasts, with common extinction at average angles of about 60–120° from the slip surface (Fig. 9A). There are also numerous, discrete rounded clasts and areas of matrix with internal domains of CPO of quartz that do not make regular angles with the slip surface consistent with observations by Power and Tullis (1989). Many of the silicified clasts have varying degrees of optical contrast with the matrix suggestive of varying degrees of silicification and

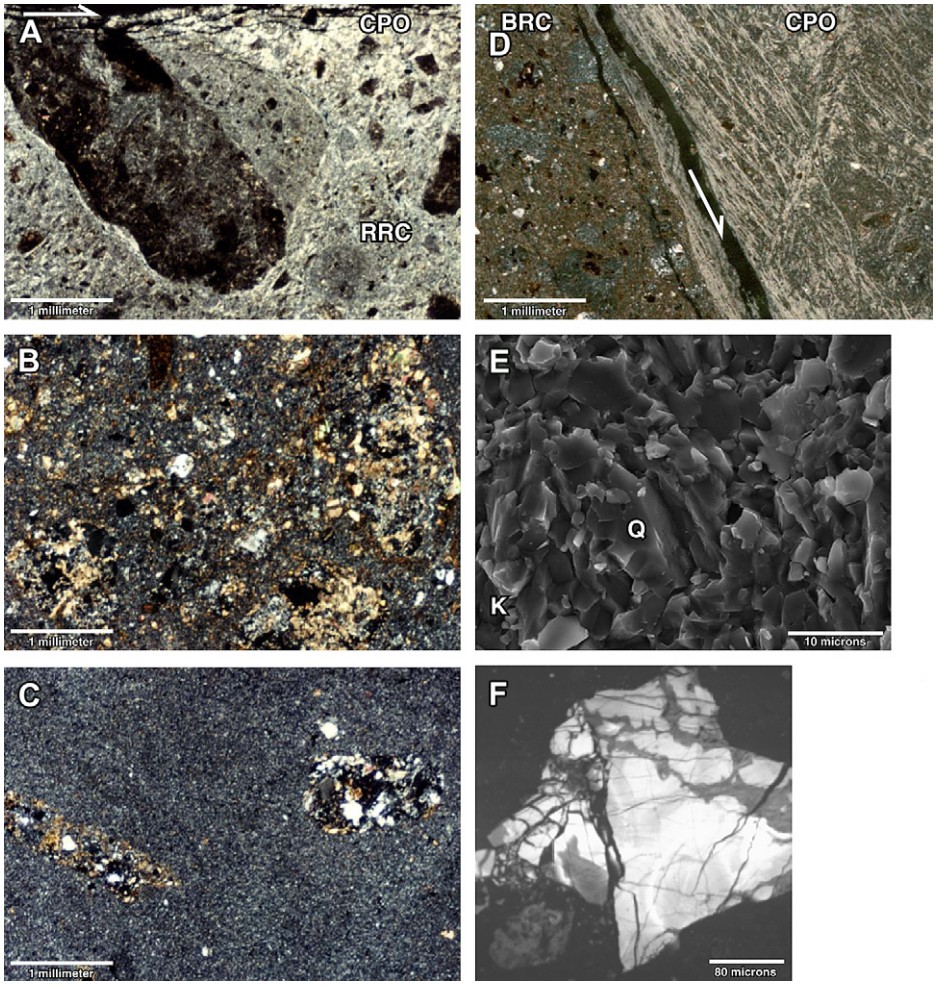

Fig. 9. Polarized light and scanning electron microscope (SEM) micrographs of the three breccias found in Fig. 8. A) Silicified breccia with rounded clasts that formed directly under a polished and striated slip surface shown by a white arrow. Note the rounded and angular clasts, completely silicified relict clasts (RRC), partially clast-supported texture, and crystallographic preferred orientation (CPO) of quartz. B) Moderately silicified predominantly clast-supported breccia showing subangular clasts and poor sorting. C) Highly silicified matrix-supported breccia characterized by angular and rounded clasts sitting in an undeformed microcrystalline, quartz-rich matrix. D) Oriented section of the sharp juxtaposition of two different breccias with rounded clasts (BRC) separated by a polished and striated silicified slip surface (the section separated along the thick dark irregular line with the white arrow in it). E) SEM, secondary electron image of the predominantly quartz (Q) matrix with minor kaolinite (K) from the hanging wall of the sample shown in D (mineralogy determined by energy dispersive spectroscopy). The image is roughly oriented as image D. F) Cathodoluminescence image of a clast within the microcrystalline quartz matrix (black background). The triangular clast is interpreted as deformed quartz and the background quartz is interpreted as undeformed quartz. Note that the clast is laced with several generations of healed microfractures (black and gray stringers of quartz).

clay mineral content that result in translucent gray to brown, layered to clotted, felt-like masses. Little to no carbonate is observed in these breccias which grades into clast-supported breccias as the polished face of the representative hand sample is traversed further down, where the carbonate content increases (Fig. 8). In other samples and exposures the breccias with rounded clasts abruptly cut clast-supported breccias or are themselves cut by discrete slip surfaces (e.g., Fig. 9D).

4.3.2. Clast-supported breccias

In outcrop and hand samples the most common fault-related breccias are the predominantly clast-supported breccias with local matrix-supported textures. These breccias have an average matrix-to-clast ratio of ~30:70. The clasts are poorly sorted, angular to subangular, show interclast veining, and are predominantly composed of silicified granodiorite protolith (Figs. 8 and 9B). These breccias show little evidence for cataclastic transport of rock, such as relative movement or rounding of clasts. This rock type is the 'background' fault rock that is cut by slip surfaces, breccias with rounded clasts, matrix-supported breccias, and breccias with open space. In some samples, clasts of brecciated protolith in the clast-supported breccias are recognized in thin section and appear brecciated multiple times. These types of textures are the exception and are found where the breccias are locally more matrix supported. Some clasts are locally incorporated into a fine-grained, quartz-rich breccia but none were observed with domains of quartz CPO. The clasts and silicic matrix are both cut by carbonate veins, which are also cut by fine-grained quartz + kaolinite veins. The latter assemblage is cut again by a set of young calcite veins. The veins commonly include clasts of the protolith, preexisting vein materials, breccias, and other fault-related rocks that show multiple brecciation events.

4.3.3. Matrix-supported breccias

Matrix-supported breccias are found in distinctive pod-like bodies and in veins that emanate from and (or) connect to other breccia bodies. These breccias are also characterized by angular breccia clasts of local wall rock that could be pieced back together if the matrix that separates them was removed. Yet, locally they have subrounded clasts of the other breccia types discussed

above, some with exotic compositions from the wall rock. In either case the clasts are generally widely separated from one another (Figs. 6, 8 and 9C). Breccias with angular clasts that can be pieced back together have been previously referred as "jigsaw puzzle" breccias and implosion or explosion breccias (cf. Sibson, 1986a; Jébrak, 1997; Power and Tullis, 1989; Mort and Woodcock, 2008). At the Mirrors, these breccias are matrix supported and the matrix has a distinctive beige color. They are poorly sorted, highly silicified, lack veins or fractures, and exhibit no open, macroscopic pore space. The breccia pods in which the matrix-supported breccias occur abruptly and irregularly cut the other breccia types (Fig. 8).

The clasts in the matrix-supported breccias range from 1 mm to 3 cm in size, contain multiple clasts of varying composition with cross cutting internal brecciation but are compositionally distinct from the beige matrix (Fig. 8). Clast size distribution is variable but most clasts are orders of magnitude larger than the matrix (Figs. 8 and 9C). Clasts generally contain deformed angular quartz grains visible in thin section. Cathodoluminescence analysis of the matrix-supported breccia samples shows extensive fracturing and multiple vein-filling events isolated within the clasts with no such deformation or veining in the matrix (Fig. 9F). Clast lithologies include adjacent wall rock breccias in the jigsaw puzzle breccias. Other clast lithologies include protolith granodiorite, porphyritic volcanic rocks, iron-stained and zoned dolomite vein crystals, relicts of highly silicified breccia clasts in contact with their matrix material, polished and striated fault surface materials, and possible metasedimentary rock fragments. Calcite occurs as intraclast vein fillings in association with ferroan dolomite and as a late-stage precipitate that fills some isolated void spaces, small stringer-like veins, and as dismembered vein fragments.

The clasts are encased in a distinctive ultra-fine-grained ($\sim$0.1–10 μm), beige colored, microcrystalline quartz-rich matrix with minor amounts of intergrown kaolinite, trace amounts of carbonate and amorphous material (Table 1). The matrix shows rather uniformly sized anhedral to subhedral interlocking quartz crystals with salt and pepper or mosaic-like microtexture (Fig. 9C). Sub-equant, poorly developed quartz prisms with anhedral quartz intergrowths are occasionally observed with somewhat reticulate texture. All quartz grains are completely intergrown and conform to every surface they are in contact with, showing no evidence for preferred crystallographic orientation, spherulitic, or feathering textures. Quartz crystals have uniform to domainal extinction within individual grains and within masses of grains. The matrix shows no evidence of brecciation, layering, overgrowths, cross-cutting veins, or crack-seal textures. Carbonate appears to fill minor void space as late-stage precipitate.

Maximum syndeformational porosity in the breccia pods was estimated from representative hand samples of the matrix-supported breccias. Syndeformation porosity was estimated by digital imaging of 'serial' sections from several slabbed and polished samples ranging in size from about 20 by 10 cm to about 3 by 5 cm (e.g., the lower part of Fig. 8). The samples were scanned and a gray-scale histogram was captured for each image where the dark histogram signal was assumed to represent the clasts and the light histogram signal assumed to represent the matrix. The measurements also assume that the matrix of these breccias represent the pore space formed during a single deformation event, consistent with it cross-cutting other main breccias types. This is also reasonable because the matrix itself is compositionally homogenous, unlike the clasts, and shows no evidence for subsequent deformation. The average, maximum syndeformation porosity from this analysis is 54 percent and the analysis confirms the largely matrix-supported texture using this pseudo three-dimensional approach.

4.3.4. Breccias with open space

At several locations in exposures of the fault core there are breccias that exhibit significant open space and vugs (Fig. 8B). These breccias include generally angular, iron oxide stained clasts of other breccia types and are clast-supported fault rocks. The volume of the interclast open space is on the order of microns to several tens of cubic centimeters. Many of the spaces are coated with banded and multilayered carbonate rinds that consist of euhedral calcite crystals that conformably overlay previous layers and the clasts. There also are euhedral carbonate veins that cut through the clasts and in some cases connect to the euhedral rinds.

4.3.5. Fault gouge

The final fault-rock category found at the Mirrors is unconsolidated fault gouge (cf. Sibson, 1977). Only one thin seam, less than 10 cm in thickness, of this material was found. The gouge is fine to medium grained and contains silicified clasts of the breccia types described above. The gouge is not clay-rich as is commonly found in some shallowly formed, brittle faults (cf. Morrow et al., 1984; Foxford et al., 1998; Heynekamp et al., 1999; Vrolijk and van der Pluijm, 1999; Aydin and Eyal, 2002). Although the exposure of gouge cuts the clast-supported breccias its temporal relationships to the other breccias types were not observed.

4.4. Internal structure of the fault core

A characteristic feature of the fault core is the occurrence of matrix-supported breccias and other fault rocks that form pod-like bodies (Figs. 3 and 6). The pods are generally lenticular with their long axes subparallel to the average orientation of the slip vector for the master fault zone. The short axes of the breccia pods are typically orthogonal to slip in the plane of the fault. Large slip surfaces have elongated scoop-like depressions and associated ridges parallel to the slip direction. The walls of the breccia pods that are not bounded by slip surfaces are irregular and where exposed, they are enveloped in fractured protolith. One pod-shaped structure shows an along-strike dimension of several meters, a down-dip dimension of $\sim$35 m, and a thickness of less than $\sim$5 m (Fig. 6). The bulk of the pod is predominantly composed of silicified clast-supported breccias with interior meter-scale pods of the beige matrix-supported breccias. This pod was one of the largest in outcrop; pods on the order of $\sim$2 m or less in length are more typical.

The dimensions of exposed curviplanar or corrugated slip surfaces that bound breccia bodies were characterized using wavelength and amplitude measurements made with a tape measure in the plane of the fault orthogonal to the slip direction. The dimensions range from a maximum of approximately 35 m in length to 3 m in amplitude at the map scale and 4 m in length to 0.5 m in amplitude at the outcrop scale. There is insufficient exposure to make full measurements of anisotropy parallel to slip at the map scale; however, at the outcrop scale on average the pods vary in length from roughly 2 m to 15 m, with length to amplitude ratios between 7:1 and 20:1. There is a difference in the wavelength to amplitude ratio of breccia body corrugations in a direction perpendicular to slip versus parallel to slip. At the outcrop scale, corrugations parallel to slip may be up to three times as long as those perpendicular to slip. In spite of the crude nature of these estimates, they are consistent with other more sophisticated measurements of fault surface roughness for the Mirrors and other localities over a number of scales (cf. Lee and Bruhn, 1996; Sagy et al., 2007).

En échelon, highly angular beige matrix-supported breccia clasts in veinlets that extend from the breccia pods, indicate wall rock fracture, shear, and subsequent fluid flow within the breccia pod interiors prior to mineral precipitation and sealing (Fig. 6).

Breccia-filled veins at the margins of the pods taper away from the pods and terminate. Some of these veins, similar to that seen in Fig. 6, are connected to an extensive network of veins that are irregularly shaped, show variable thickness, and extend into the damage zone.

5. Discussion

The SFZ at the Mirrors locality comprises a complex set of structures and rock types that include multiple slip surfaces, distinct fault rocks and breccia bodies, fault and non-fault-related fracture networks. We infer that several processes acted together during the formation of the fault zone and that some of the rocks may record coseismic deformation and associated fluid flow. In the following discussion we present key observations and a conceptual model that links deformation and fluid flow to architecture, permeability structure, and fault-zone growth.

5.1. Origin of the breccias and breccia pods

The key observations and interpretations that bear on the origin of the different breccia types and breccia pods as recording coseismic processes, and the growth of the SFZ include the following. The breccia pods are discontinuous, elongate, and tapered bodies aligned subparallel to the slip direction of the master fault zone. These pods are primarily composed of clast-supported breccias with local matrix-supported breccias. Silicified slip surfaces and associated breccias with rounded clasts cut the clast-supported breccias but are also locally brecciated. The matrix-supported breccias are emplaced into the surrounding clast-supported breccias, slip surfaces, and breccias with rounded clasts within the pods. Pod morphology, spatial restriction to the fault core, kinematic compatibility with normal faulting, and large estimated syndeformational porosity of the matrix-supported breccias suggest that there was a component of dilatational strain during deformation and pod formation. Slip surfaces and some matrix-supported breccias with en échelon clasts also record a component of shear deformation.

The topography of many of the large slip surfaces that bound the pods includes elongated scoop-like depressions that may have formed along local extensional fault jogs. These relatively small-scale depressions may also record local dilatational strain and permeability enhancement during coseismic deformation (e.g., Power and Tullis, 1989). Sibson (1986a) inferred that brecciation could be caused by pore fluid-pressure differentials between the wall rock and an incipient, dilatant opening within a fault zone. If the effective stress acting on a fault zone exceeds the tensile strength of the wall rock, catastrophic failure can cause 'implosion' of the wall rock into openings. Many of the breccia pods, however, do not occur near slip surfaces and are larger than openings due to different topography along adjacent slip surfaces. This, and the fault-slip parallel morphology of the larger breccia pods, suggests that some pods may have originated by processes other than dilatational strain in jogs caused by variations in slip-surface topography. These larger breccia pods may have formed along mechanically weak sites within the fault core such as preexisting polished and striated slip surfaces, macroscopic fractures that were partially mineral-filled, microfractured regions, or zones of compositional variation.

The clast-within-clast textures found in the breccias provide a record of multiple faulting or slip events localized in the core. The matrix-supported jigsaw puzzle breccias have clasts that are composed of the adjacent wall rock and these are generally angular suggesting little transport. However, locally in the breccia pods, where there are widely separated clasts in the same matrix as the jigsaw puzzle breccias, the clasts are composed of exotic parent lithologies and are subangular to subrounded indicating significant transport. The rounded clasts may also indicate mechanical attrition from grain-size reduction given their proximity to slip surfaces. Clast rounding may also have occurred during hydrothermal fluid flow and associated abrasional wear of clasts against one another in saturated, silica-rich rock flour (cf. Sillitoe, 1985; Jébrak, 1997).

The matrix of breccia pods with matrix-supported clasts is composed of distinctive beige colored, homogenous, fine-grained, quartz with minor kaolinite and carbonate. The quartz has a mosaic texture with uniformly sized ($\sim$0.1–10 μm) anhedral to subhedral interlocking crystals that form domains of variable optical extinction and that completely infill and conform to all available space. Lovering (1972), Fournier (1985), Saunders (1994), and Dong et al. (1995) provide evidence that this mosaic texture forms by recrystallization of amorphous silica that precipitated from the boiling of hydrothermal fluids and associated processes at temperatures $<$180 °C. At the temperatures of the modern geothermal reservoir, a rapid pressure drop could result in such decompressional (isoenthalpic) boiling, phase separation, cooling, and rapid precipitation of amorphous silica (Hedenquist and Henley, 1985; Saunders, 1994; Rimstidt, 1997). Such pressure drops could have occurred in seismically induced dilatant openings localized in the fault zone (e.g., Sibson, 1986a) and that could have also hydraulically connected the reservoir to the surface. Decompressional boiling is consistent with the minor kaolinite and carbonate minerals found in small interstices of the mosaic quartz matrix. These phases are also found in fault rocks elsewhere along the SFZ (Parry et al., 1991). Loss of CO_2 to the vapor phase during boiling, with attendant increase in pH, will cause clay and carbonate to precipitate (e.g., Fournier, 1985). Such decompression coupled with rapid amorphous silica deposition required rapid flow of fluid and vapor up through, and laterally within, the fault zone. Surficial expression of this type of fluid movement is evident as sinter mounds and terraces, hot springs, and fumaroles such as those found at the ground surface in association with the fault zone (cf. Caine and Forster, 1999; Lutz et al., 2002).

Breccia-filled veins, with the same quartz–kaolinite matrix as the breccia pods emanate from and taper outward from the pod margins and terminate. This may indicate that fluid flow and the pressure gradient were directed outward from the pod interior. The pods then likely became permeability heterogeneities within the fault core leading to a heterogeneous spatial distribution of 'cemented' or sealed portions of the fault zone. This, in turn, may have lead to heterogeneities in fault-zone strength as the fault zone evolved.

Observations of the juxtaposition of polished slip surfaces against breccias with rounded clasts, cutting across clast-supported breccias with angular clasts, then cut by matrix-supported breccias with jigsaw puzzle and rounded clasts, open space breccias, the irregular character of some of the larger breccia-filled veins, and a seam of clay-rich gouge indicate that different mechanisms of failure may have been operative in the fault zone over time. Some of these mechanisms may be attributed to a non-static stress field changing dynamically during deformation or attributed to variations in fluid pressures within the fault zone at different times (cf. Caskey and Wesnousky, 1997; Micklethwaite, 2009). Multiple, anastomosing, layered slip surfaces with curviplanar geometry and different lineation directions indicate some portion of slip during any deformation event was distributed along any number of preexisting surfaces from previous events. However, no evidence was found to evaluate the nature of the actual slip distribution on an event-by-event basis.

If breccia pod formation was seismogenic, it is unclear if they are related to hypocentral earthquake nucleation sites or possibly

record rupturing in more distal and shallower parts of the fault zone. The breccia pods and associated rocks may be unique remnants of the deformation products linked to the distribution of earthquake foreshocks, aftershocks, and microseismicity as rupturing initiated and ceased, and pore pressure adjusted to structural changes throughout the fault zone (cf. Nur and Booker, 1972; Byerlee, 1993; Miller et al., 1996, 2004). Episodic deformation and resulting fault rocks evolved into a hydraulically heterogeneous fault zone with local permeability contrasts great enough to possibly have trapped fluids under varying pressures. Byerlee (1993) proposed a 'fluid-pressure compartment' model for fault zones associated with earthquakes where fluid sealed under high pressure in hydraulically isolated compartments partially drains into adjacent compartments of initially lower fluid pressure during a deformation event. Although not a direct comparison, Parry and Bruhn (1990) and Parry et al. (1991) showed evidence for transient variations in fluid pressure from fluid inclusion data from the SFZ about 40 km south of the Mirrors locality. The breccia pods are not likely remnants of Byerlee-like pressure compartments per se, however, the locations, sizes, shapes, and breaching of the breccia pods were likely influenced by variations in permeability, pore fluid pressure, and mechanical heterogeneities; features that may also help to explain the variable fluid pressures observed by Parry and Bruhn (1990).

5.2. Heterogeneity and anisotropy within the fault zone

Several types of structural heterogeneities and anisotropies may act together to impact fluid flow, mechanics, and growth of the SFZ. Fault-related permeability anisotropy in crystalline rock is controlled by fracture networks and heterogeneously distributed fault-rock types, such as the breccia bodies, with varying permeabilities (e.g., Seront et al., 1998; Caine and Forster, 1999). The corrugated topography of the major slip surfaces that bound the fault core and minor slip surfaces within the fault core may have had a role in controlling the shapes and limited the growth of breccia bodies. The elongation of these bodies parallel to the slip direction should also contribute to permeability heterogeneity. Anisotropic slip-surface topography may also be an important cause of changes in local stress fields (Ferrill et al., 1999). The distribution of slip surface and slip vector orientation data suggests that most of the oblique slip is related to the accommodation of deformation along the corrugated slip surfaces consistent with attendant localized changes in the local stress field (Fig. 5).

Outcrop-scale fracture network heterogeneities, such variations in total fracture intensity between the damage zone and protolith, the apparent unsystematic manner in which fracture intensity changes with distance from the fault core, or internal heterogeneity of the number of shear fractures and minor slip surfaces in any given location, suggest that deformation and slip for any given deformation event were heterogeneously distributed. Thus, fault properties such as strain, strength, and permeability depend on the range of scales over which fault-rock and damage-related heterogeneities exist. For example, the elongate nature of the bodies of fault-core breccias, the contrast of fracture network intensity between the fault core and damage zone, and the variable degree of silica cementation in the fracture networks are evidence of significant hydrogeologic and mechanical heterogeneities and anisotropies, implying there is significant heterogeneity of fault-zone strength and permeability from at least the outcrop scale to the map scale.

Seront et al. (1998) measured permeability values on representative core-plug samples that ranged from as high as 10^{-8} m^2 in the damage zone to as low as 10^{-20} m^2 in the fault-core matrix. Given the map-scale to micro-scale change in fracture intensity is higher in the damage zone than in the fault core and that the core is the locus of silicification, a heterogeneous combined conduit-barrier permeability structure is suggested for the fault zone during interseismic periods (cf. Caine and Forster, 1999). Although speculative, this permeability heterogeneity could also lead to pore-pressure heterogeneity and consequently strength heterogeneity throughout the seismic cycle.

Seront et al. (1998) also found no appreciable difference in mechanical strength of small laboratory samples of each fault-zone component at the Mirrors. Their experimental results highlight the importance of scale when considering the relative mechanical strength within a fault zone composed of discrete components. For example, uncemented, smooth-walled and discontinuous shear fractures observed along the fault-core/damage-zone contact, and within the damage zone, would provide favorably oriented failure surfaces for later deformation and fluid flow events (e.g., Barton et al., 1997). The mechanical strength of these macro-scale fractures would depend on frictional properties of the fractures rather than grain-scale cohesion or microfracture properties that control strength at the core-plug scale.

5.3. Model for deformation induced fluid flow

We propose the following conceptual model that relates deformation, growth, fault-related fluid flow, and stress cycling to architecture and permeability structure (Fig. 10). The proposed model is built on the work of Power and Tullis (1989), Parry and Bruhn (1990), Parry et al. (1991), Muir-Wood (1994), Seront et al. (1998), and Sibson (2001) and assumes a constant maximum and decreasing minimum principal stress in an Andersonian normal fault regime.

During interseismic periods, fluids were stored in an ancient equivalent of the modern geothermal reservoir, in primary pore space, and secondary macroscopic fracture networks in and surrounding the fault zone (Fig. 10). The hydrothermal silica cements in the fault core were likely precipitated from fluids that initially equilibrated with rocks in this reservoir. Aseismic deformation along slip surfaces may have occurred as hypothesized by Power and Tullis (1989). As differential stress increased, preexisting fractures primarily in the damage zone, could have opened due to decreasing minimum compressive stress. New fractures may also have formed which mobilized fluids and possibly dissolved silica from comminuted by-products formed in preexisting fractures in the surrounding host rock.

During coseismic brittle failure events new hydraulic connections to the geothermal reservoir were formed as ruptures propagated likely releasing seismic energy. Quartz-supersaturated fluid and vapor infiltration, flow, boiling and (or) phase separation occurred in these new, highly permeable pathways (cf. Miller et al., 2004). This resulted in rapid quartz matrix precipitation and suspension of clasts forming the matrix-supported breccias in hybrid dilatant and shear related openings localized in the fault core. The effective minimum compressive stress also increased, closing optimally oriented damage-zone fractures further mobilizing fluids into the fault core with accompanying shear along both preexisting and newly formed discrete fractures and fracture networks (cf. Muir-Wood and King, 1993; Seront et al., 1998; Fig. 10). Comminution and the development of breccias with rounded clasts were localized along constrictions between discrete slip surfaces. Adjacent to slip surfaces and in the wall rock, *in situ* distributed failure, possibly crushing, resulted in predominantly clast-supported breccias. Some of the clast-supported breccias with localized areas of matrix-supported textures may be older equivalents of breccias similar to the beige matrix-supported breccias. This process appears to have been repeated numerous times and

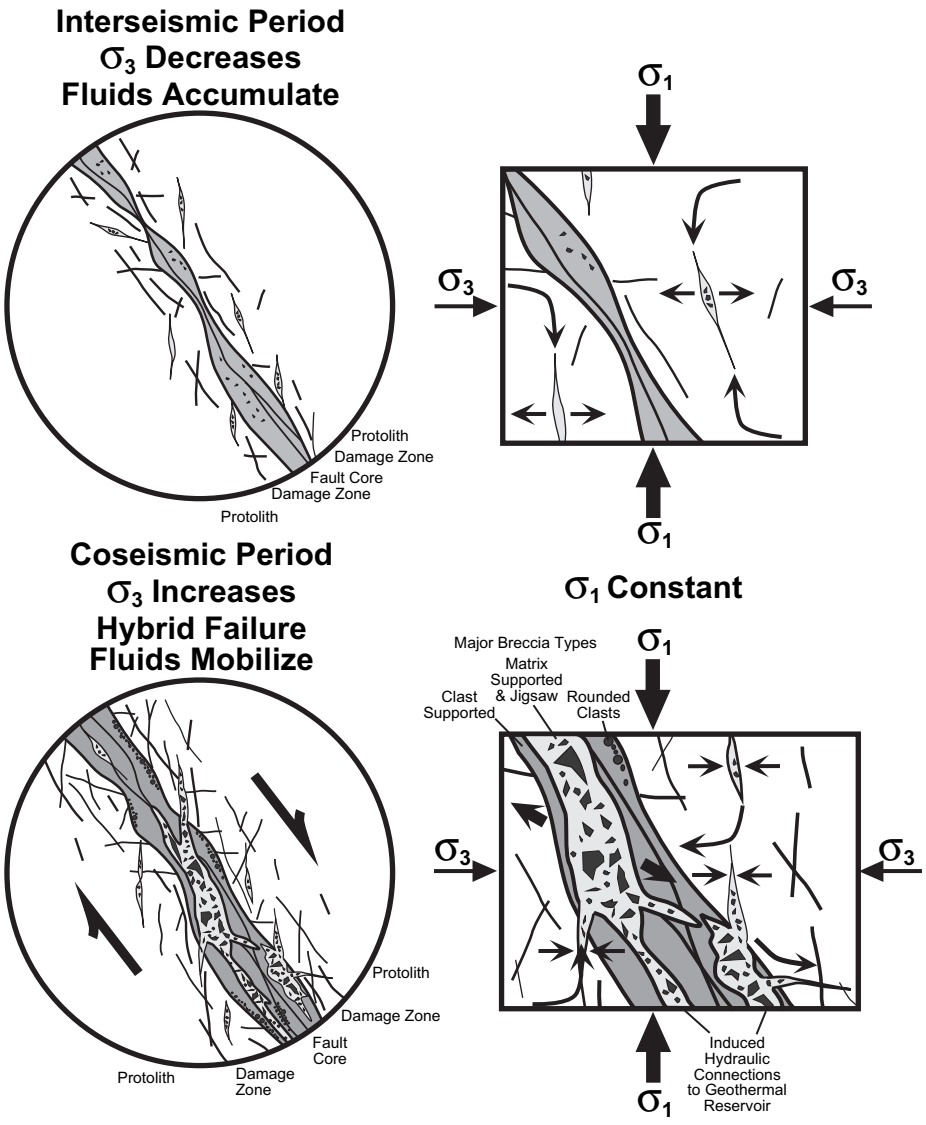

Fig. 10. Schematic diagram and conceptual model of deformation, breccia formation, hybrid shear and dilatant fault growth, and fluid flow inferred from the Mirrors locality (hydrologic effects adapted from Muir-Wood, 1994 and specific structures from this work). The regional maximum principal stress (σ_1) is assumed to be constant and vertical throughout the evolution of the fault zone. The minimum principal stress (σ_3) is assumed to be horizontal. At an early time (top diagram) in its evolution, the fault core is predominantly composed of clast-supported breccias cut by breccias with rounded clasts (middle gray fill) and associated anastomosing slip surfaces (black lines that bound and weave through the fault core). In the interseismic period when σ_3 decreases as differential stress increases, optimally oriented fracture networks dilate (stubby arrows indicate local stress), take on and store fluids (curved arrows indicate fluid transport direction). During a coseismic period, mixed-mode deformation (shear and dilatancy) is localized in the fault core creating new hydraulic connections to an ancient geothermal reservoir accompanied by fluid flow into breccia pods (light gray fill), development of breccias with rounded clasts, and rapid precipitation of quartz due to decompressional boiling, locally sealing the fault zone. Because effective σ_3 is increased, fluids may also flow into the high permeability fault core from optimally oriented damage-zone fracture networks.

may have resulted in an increase in width of the fault zone as well as heterogeneous sealing of the fault core. Dilatancy hardening may also have resulted in association with fluid-pressure drops (cf. Parry et al., 1991).

Alternatively, the formation of the matrix-supported breccias in discrete pods and some of the clast-supported breccias may have formed by the fault-valve mechanism (Sibson, 1990) where failure was driven by pore fluid pressure rather than tectonic stress. The present geothermal reservoir near the Mirrors locality appears to be in a heterogeneous pressure regime largely at or near hydrostatic pressure but with areas of enhanced pressure (Hickman et al., 2000). Whereas, deep wells drilled outside of the productive geothermal reservoir have artesian pressures (Dick Benoit, personal communication, 2009). It may have been possible that there were volumes of the ancient reservoir with localized areas of overpressure connected to the fault zone or zones within the fault with anomalous fluid pressures possibly due to permeability heterogeneity as suggested above. In either case, the various breccia textures do not provide unique evidence for a tectonic stress versus pore fluid-pressure mechanism for their origin.

Exhumation of the Mirrors portion of the fault zone brought the fault zone into progressively different temperature, pressure, and fluid chemical conditions. The breccias with open space may have originated from low pH ascending fluids and yet clasts coated with euhedral carbonate rinds are consistent with downwelling, silica undersaturated fluids both possible processes during interseismic periods. Cross-cutting seams of fault gouge like represent yet another phase of deformation largely lacking significant localized fluid flow and associated hydraulic connection.

6. Conclusions

Field mapping along the Stillwater Fault Zone provides a detailed view of the internal structure of the footwall of a seismogenic normal fault zone. Distinct mechanical and hydraulic components include a fault core, damage zone, and protolith (cf. Seront et al., 1998). The different components are distinguished by distinctive variations in lithology, amount and type of hydrothermal alteration, fracture intensity, matrix-scale hydraulic properties, and structure. The fault core shows evidence for localized deformation along silicified slip surfaces near large dilatant breccia pods indicative of distributed deformation (cf. Power and Tullis, 1989). The core is surrounded by damage-zone fracture networks also indicative of distributed deformation. The juxtaposition of these distinct deformational styles leads us to characterize the architecture of the fault zone at the Mirrors locality as a composite deformation zone (Caine and Forster, 1999) where different fault-related breccias and other fault rocks are indicative of multiple deformation events possibly under different stress and (or) fluid-pressure conditions as the fault zone evolved.

Laboratory-derived permeability values indicate up to approximately four orders of magnitude difference in permeability between the fault rock, damage zone, and protolith samples at the core-plug scale. This and fracture network modeling (Caine and Forster, 1999) in combination with the mapped fault-zone components lead us to infer that the bulk permeability structure of the present day fault zone is a heterogeneous and anisotropic combined conduit-barrier flow system (e.g., Caine et al., 1996). During seismic events, much of the fault zone behaves as a complex and heterogeneous conduit where flow paths are likely controlled to a large degree by mechanical heterogeneities, and the local stresses they may induce (e.g., Faulkner et al., 2006). These heterogeneous features are formed during progressive deformation and associated sealing events. The source of fluids, fluid temperatures, and component chemical constituents also play a large role in the distribution of permeability and mechanical heterogeneity from one seismic cycle to another.

The breccia pods contain remnants of likely coseismic, outcrop to map-scale openings with components of hybrid dilatant and shear deformation. Distinctive matrix-supported and jigsaw puzzle breccias within these pods have microcrystalline, quartz-rich mosaic textures that may record rapid, hydrothermal fluid flow and mineral precipitation induced by the coseismic dilatancy and hydraulic connection to an ancient geothermal reservoir. Alternatively, the matrix-supported breccias and associated pods may have formed from fluid overpressures either in connection with the geothermal reservoir or locally within the core of the fault. In either case, the various breccia textures do not provide unique evidence for a tectonic stress versus pore fluid-pressure mechanism for their origin. Yet, if either hypothesis is correct, these distinctive fault rocks are formed during high enough strain rates to qualify as being coseismic, and thus the breccias represent seismogenic rock textures (cf. Cowan, 1999). Although, the fault rocks at the Mirrors locality may be coincidental and unique to the Stillwater Fault Zone, the textures and associated inferences regarding their formation may be underappreciated where similar combinations of rocks, structures, and geothermal fluid reservoirs occur.

Acknowledgements

Funding for this work was provided by a U.S. Geological Survey, National Earthquake Hazards Reduction Program Grant # 1434-93-G-2280 to Forster and Bruhn who supported Caine with a graduate research assistantship at the University of Utah, Department of Geology and Geophysics from 1992 through 1995. We thank Bill Parry, Laurel Goodwin, Darrel Cowan, George Breit, Don Sweetkind, and Albert Hofstra, for helpful comments on an early version of this manuscript. Lyndsay Ball, Dan Faulkner, David Lockner, Steven Micklethwaite, and Rick Sibson provided critical reviews that greatly improved the manuscript. We also thank Bennet Leeper, Lori Chadwell, Kathleen Royster, and Bernard Seront who provided field assistance.

References

Antonellini, M., Aydin, A., 1994. Effect of faulting on fluid flow in porous sandstones; petrophysical properties. AAPG Bulletin 78, 355–377.

Aydin, A., Eyal, Y., 2002. Anatomy of a normal fault with shale smear; implications for fault seal. AAPG Bulletin 86 (8), 1367–1381.

Barton, C.A., Hickman, S., Morin, R., Zoback, M.D., Finkbeiner, T., Sass, J., Benoit, W.R., 1997. Fracture permeability and its relationship to in-situ stress in the Dixie Valley, Nevada, geothermal reservoir. Report SGP-TR-155. In: Proceedings of the 22nd Workshop on Geothermal Reservoir Engineering. Stanford University, Stanford, California, pp. 147–152.

Bruhn, R.L., Yonkee, W.A., Parry, W.T., 1990. Structural and fluid-chemical properties of seismogenic normal faults; earthquake source processes. In: 19th IUGG General Assembly, Symposium on Earthquake Source Processes, Vancouver, BC, Canada, Aug. 19–21, 1987, vol. 175, pp. 139–157.

Bruhn, R.L., Perry, W.T., Yonkee, W.A., Thompson, T., 1994. Fracturing and hydrothermal alteration in normal fault zones; faulting, friction, and earthquake mechanics; part 1. Pure and Applied Geophysics 142, 609–644.

Byerlee, J.D., 1993. Model for episodic flow of high-pressure water in fault zones before earthquakes. Geology 21, 303–306.

Caine, J.S., Evans, J.P., Forster, C.B., 1996. Fault zone architecture and permeability structure. Geology 24, 1025–1028.

Caine, J.S., Forster, C.B., 1999. Fault zone architecture and fluid flow; insights from field data and numerical modeling. In: Haneberg, W.C., Mozley, P.S., Moore, J.C., Goodwin, L.B. (Eds.), Faults and Sub-surface Fluid Flow in the Shallow Crust. AGU Geophysical Monograph, vol. 113, pp. 101–127.

Caskey, S.J., Wesnousky, S.G., Zhang, P., Slemmons, D.B., 1996. Surface faulting of the 1954 Fairview Peak (M_S 7.2) and Dixie Valley (M_S 6.8) earthquakes, central Nevada. Bulletin of the Seismological Society of America 86, 761–787.

Caskey, S.J., Wesnousky, S.G., 1997. Static stress changes and earthquake triggering during the 1954 Fairview Peak and Dixie Valley earthquakes, central Nevada. Bulletin of the Seismological Society of America 87 (3), 521–527.

Chester, F.M., Evans, J.P., Biegel, R.L., 1993. Internal structure and weakening mechanisms of the San Andreas Fault. Journal of Geophysical Research 98 (B1), 771–786.

Chester, F.M., Logan, J.M., 1986. Implications for mechanical properties of brittle faults from observations of the Punchbowl fault zone, California. Pure and Applied Geophysics 124, 79–106.

Cowan, D.S., 1999. Do faults preserve a record of seismic slip? A field geologist's opinion. Journal of Structural Geology 21, 995–1001.

Cox, S.F., Knackstedt, M.A., Braun, J., 2001. Principles of structural control on permeability and fluid flow in hydrothermal systems. Reviews in Economic Geology 14, 1–24.

Dong, G., Morrison, G., Jaireth, S., 1995. Quartz textures in epithermal veins, Queensland; classification, origin and implication. Economic Geology and the Bulletin of the Society of Economic Geologists 90, 1841–1856.

Evans, J.P., Chester, F.M., 1995. Fluid–rock interaction in faults of the San Andreas system: inferences from San Gabriel fault rock geochemistry and microstructures. Journal of Geophysical Research 100 (B7), 13007–13020.

Faulkner, D.R., Mitchell, T.M., Healy, D., Heap, M.J., 2006. Slip on 'weak' faults by the rotation of regional stress in the fracture damage zone. Nature 444, 922–925.

Faulkner, D.R., Mitchell, T.M., Rutter, E.H., Cembrano, J., 2008. On the structure and mechanical properties of large strike–slip faults. In: Wibberley, C.A.J., Kurz, W., Imber, J., Holdsworth, R.E., Collettini, C. (Eds.), The Internal Structure of Fault Zones: Implications for Mechanical and Fluid Flow Properties. Geological Society, London, Special Publications, vol. 299, pp. 139–150.

Ferrill, D.A., Stamatakos, J.A., Sims, D., 1999. Normal fault corrugation; implications for growth and seismicity of active normal faults. Journal of Structural Geology 21, 1027–1038.

Forster, C.B., Evans, J.P., Torgersen, T., 1991. Hydrogeology of thrust faults and crystalline thrust sheets; results of combined field and modeling studies. Geophysical Research Letters 18, 979–982.

Fournier, R.O., 1985. The behavior of silica in hydrothermal solutions. In: Berger, B.R., Bethke, P.M. (Eds.). Geology and Geochemistry of Epithermal Systems. Reviews in Economic Geology 2, 45–61. Society of Economic Geologists.

Foxford, K.A., Walsh, J.J., Watterson, J., Garden, I.R., Guscott, S.C., Burley, S.D., 1998. Structure and content of the Moab Fault Zone, Utah, USA, and its implications for fault seal prediction. In: Jones, G., Fisher, Q.J., Knipe, R.J. (Eds.), Faulting, Fault Sealing, and Fluid Flow in Hydrocarbon Reservoirs. Geological Society, London, Special Publications, vol. 147, pp. 87–103.

Ghisetti, F., Kirschner, D., Vezzani, L., Agosta, F., 2001. Stable isotope evidence for contrasting paleofluid circulation in thrust faults and normal faults of the central Apennines, Italy. Journal of Geophysical Research 106, 8811–8825.
Goddard, J.V., Evans, J.P., 1995. Chemical changes and fluid–rock interaction in faults of crystalline thrust sheets, northwestern Wyoming, U.S.A. Journal of Structural Geology 17, 533–547.
Hancock, P.L., Barka, A.A., 1987. Kinematic indicators on active normal faults in western Turkey. Journal of Structural Geology 9, 573–584.
Hedenquist, J.W., Henley, R.W., 1985. Hydrothermal eruptions in the Waiotapu geothermal system, New Zealand; their origin, associated breccias, and relation to precious metal mineralization. Economic Geology and the Bulletin of the Society of Economic Geologists 80, 1640–1668.
Heynekamp, M.R., Goodwin, L.B., Mozley, P.S., Haneberg, W.C., 1999. Controls on fault-zone architecture in poorly lithified sediments, Rio Grande Rift, New Mexico; implications for fault-zone permeability and fluid flow; faults and subsurface fluid flow in the shallow crust. Geophysical Monograph 113, 27–49.
Hickman, S.H., Barton, C.A., Zoback, M.D., Morin, R., Sass, J.H., Benoit, R., 1997. In situ stress and fracture permeability along the Stillwater fault zone, Dixie Valley, Nevada. International Journal of Rock Mechanics and Mining Sciences & Geomechanics Abstracts 34, 414.
Hickman, S.H., Barton, C.A., Zoback, M.D., Morin, R.H., Benoit, R., et al., 1998. In-situ stress and fracture permeability along the Stillwater fault zone, Dixie Valley, Nevada. Eos, Transactions, American Geophysical Union 79, 814.
Hickman, S.H., Zoback, M.D., Barton, C.A., Benoit, R., Svitek, J., Summers, R., 2000. Stress and permeability heterogeneity within the Dixie Valley geothermal reservoir: recent results from well. Report SGP-TR-165. In: Proceedings of the 25th Workshop on Geothermal Reservoir Engineering. Stanford University, Stanford, California, pp. 82–85.
Hubbert, M.K., Rubey, W.W., 1959. Mechanics of fluid-filled porous solids and its application to overthrust faulting, [part] 1 of role of fluid pressure in mechanics of overthrust faulting. Geological Society of America Bulletin 70, 115–166.
Jébrak, M., 1997. Hydrothermal breccias in vein-type ore deposits; a review of mechanisms, morphology and size distribution. Ore Geology Reviews 12 (3), 111–134.
Keller, E.A., Loaiciga, H.A., 1993. Fluid-pressure induced seismicity at regional scales. Geophysical Research Letters 20, 1683–1686.
Knipe, R.J., Jones, G., Fisher, Q.J., 1998. Faulting, fault sealing and fluid flow in hydrocarbon reservoirs: an introduction. In: Jones, G., Fisher, Q.J., Knipe, R.J. (Eds.), Faulting, Fault Sealing, and Fluid Flow in Hydrocarbon Reservoirs. Geological Society, London, Special Publications, vol. 147, pp. vii–xxi.
Lee, J.-J., Bruhn, R.L., 1996. Structural anisotropy of normal fault surfaces. Journal of Structural Geology 18, 1043–1059.
Lockner, D.A., Tanaka, H., Ito, H., Ikeda, R., Omura, K., Naka, H., 2009. Geometry of the Nojima fault at Nojima-Hirabayashi, Japan – I. A simple damage structure inferred from borehole core permeability. Pure and Applied Geophysics 30, 1649–1667.
Lovering, T.G., 1972. Jasperoid in the United States; Its Characteristics, Origin, and Economic Significance. U.S. Geological Survey Professional Paper, Report: P 0710, 164 pp.
Lutz, S.J., Moore, J.N., Benoit, D., 1997. Geologic framework of Jurassic reservoir rocks in the Dixie Valley geothermal field, Nevada: implications from hydrothermal alteration and stratigraphy. Proceedings – Workshop on Geothermal Reservoir Engineering 155, 131–139.
Lutz, S.J., Caskey, S.J., Mildenhall, D.C., Browne, P.R.L., Johnson, S.D., 2002. Dating sinter deposits in northern Dixie Valley, Nevada; the paleoseismic record and implications for the Dixie Valley geothermal system. Proceedings – Workshop on Geothermal Reservoir Engineering 171, 284–290.
Martel, S.J., 1990. Formation of compound strike–slip fault zones, Mount Abbot Quadrangle, California. Journal of Structural Geology 12, 869–882.
Micklethwaite, S., 2009. Mechanisms of faulting and permeability enhancement during epithermal mineralisation; Cracow goldfield, Australia. Journal of Structural Geology 31 (3), 288–300.
Miller, S.A., Nur, A., Olgaard, D.L., 1996. Earthquakes as a coupled shear stress – high pore pressure dynamical system. Geophysical Research Letters 23, 197–200.
Miller, S.A., Collettini, C., Chiaraluce, L., Cocco, M., Barchi, M., Kaus, B.J.P., 2004. Aftershocks driven by a high-pressure CO_2 source at depth. Nature 427, 724–727.
Morrow, C.A., Shi, L.Q., Byerlee, J.D., 1984. Permeability of fault gouge under confining pressure and shear stress. Journal of Geophysical Research 89 (B5), 3193–3200.
Mort, K., Woodcock, N.H., 2008. Quantifying fault breccia geometry: Dent Fault, NW England. Journal of Structural Geology 30, 701–709.
Muir-Wood, R., King, G.C.P., 1993. Hydrological signatures of earthquake strain. Journal of Geophysical Research 98 (B12), 22035–22068.
Muir-Wood, R., 1994. Earthquakes, strain-cycling and the mobilization of fluids. In: Geological Society, London, Special Publications, vol. 78 85–98.
Nemcok, M., Henk, A., Gayer, R.A., Vandycke, S., Hathaway, T.M., 2002. Strike–slip fault bridge fluid pumping mechanism: insights from field-based palaeostress analysis and numerical modeling. Journal of Structural Geology 24, 1885–1901.
Newhouse, W.H., 1942. Ore Deposits as Related to Structural Features. Hafner Publishing Co., New York, London, 280 pp.
Nur, A., Booker, J.R., 1972. Aftershocks caused by pore fluid flow? Science 175, 885–887.
Page, B.M., 1965. Preliminary geologic map of a part of the Stillwater Range, Churchill County, Nevada. In: Map 28-Nevada Bureau of Mines and Geology.
Parry, W.T., Bruhn, R.L., 1990. Fluid pressure transients on seismogenic normal faults. Tectonophysics 179, 335–344.
Parry, W.T., Hedderly-Smith, D., Bruhn, R.L., 1991. Fluid inclusions and hydrothermal alteration on the Dixie Valley fault, Nevada. Journal of Geophysical Research 96 (B12), 19733–19748.
Power, W.L., Tullis, T.E., 1989. The relationship between slickenside surfaces in fine-grained quartz and the seismic cycle. Journal of Structural Geology 11, 879–893.
Priest, S., 1993. Discontinuity Analysis for Rock Engineering. Chapman and Hall.
Rice, J.R., 1992. Fault stress states, pore pressure distributions, and the weakness of the San Andreas Fault. In: Evans, B., Wong, T.-F. (Eds.), Fault Mechanics and Transport Properties of Rocks; a Festschrift in Honor of W.F. Brace. Academy Press, pp. 475–503.
Rimstidt, J.D., 1997. Gangue mineral transport and deposition. In: Barnes, H.L. (Ed.), Geochemistry of Hydrothermal Ore Deposits. John Wiley & Sons, New York, NY, pp. 487–516.
Sagy, A., Brodsky, E.E., Axen, G.J., 2007. Evolution of fault-surface roughness with slip. Geology 35, 283–286.
Saunders, J.A., 1994. Silica and gold textures in bonanza ores of the Sleeper Deposit, Humboldt County, Nevada; evidence for colloids and implications for epithermal ore-forming processes. Economic Geology and the Bulletin of the Society of Economic Geologists 89, 628–638.
Scholz, C.H., 2002. The Mechanics of Earthquakes and Faulting, second ed. Cambridge University Press, Cambridge.
Seront, B., Wong, T.-F., Caine, J.S., Forster, C.B., Bruhn, R.L., Fredrich, J.T., 1998. Laboratory characterization of hydromechanical properties of a seismogenic normal fault system. Journal of Structural Geology 20, 865–881.
Sibson, R.H., 1977. Fault rocks and fault mechanisms. Journal of the Geological Society of London 133, 191–213.
Sibson, R.H., 1981. Fluid flow accompanying faulting; field evidence and models. In: Simpson, D.W., Richards, P.G. (Eds.), Maurice Ewing Series, no.4, pp. 593–603.
Sibson, R.H., 1986a. Brecciation processes in fault zones; inferences from earthquake rupturing. Pure and Applied Geophysics 124, 159–175.
Sibson, R.H., 1986b. Earthquakes and rock deformation in crustal fault zones. Annual Review of Earth and Planetary Sciences 14, 149–175.
Sibson, R.H., 1990. Conditions for fault-valve behaviour. In: Knipe, R.J., Rutter, E.H. (Eds.), Geological Society, London, Special Publications, vol. 54, pp. 15–28.
Sibson, R.H., 1992. Implications of fault-valve behaviour for rupture nucleation and recurrence. In: Mikumo, T., Aki, K., Ohnaka, M., Ruff, L.J., Spudich, P.K.P. (Eds.), Earthquake Source Physics and Earthquake Precursors. Tectonophysics 211, 283–293.
Sibson, R.H., 1996. Structural permeability of fluid-driven fault-fracture meshes. Journal of Structural Geology 18, 1031–1042.
Sibson, R.H., 2001. Seismogenic framework for hydrothermal transport and ore deposition. Reviews in Economic Geology 14, 25–50.
Sillitoe, R.H., 1985. Ore-related breccias in volcanoplutonic arcs. In: Sawkins, F.J., Sillitoe, R.H. (Eds.), Economic Geology and the Bulletin of the Society of Economic Geologists, 80. Economic Geology Publishing Company, Lancaster, pp. 1467–1514.
Smith, L., Forster, C., Evans, J., 1990. Interaction of fault zones, fluid flow, and heat transfer at the basin scale. In: Neuman, S.P., Neretnieks, I. (Eds.), Hydrogeology, vol. 2, pp. 41–67.
Smith, S.A.F., Collettini, C., Holdsworth, R.E., 2008. Recognizing the seismic cycle along ancient faults: CO_2-induced fluidization of breccias in the footwall of a sealing low-angle normal fault. Journal of Structural Geology 30, 1034–1046.
Speed, R.C., Armstrong, R.L., 1971. Potassium–argon ages of some minerals from igneous rocks of western Nevada. Isochron/West 1, 1–8.
Speed, R.C., 1976. Geologic Map of the Humboldt Lopolith and Surrounding Terrane, Nevada.
Tanaka, H., Hinoki, S.-I., Kosaka, K., Lin, A., Takemura, K., Murata, A., Miyata, T., Shimamoto, T., Fujimoto, K., Wibberley, C.A.J., 2001. Deformation mechanics and fluid behavior in a shallow, brittle fault zone during coseismic and interseismic periods; results from drill core penetrating the Nojima Fault, Japan. Island Arc 10, 381–391.
Ujiie, K., Yamaguchi, A., Kimura, G., Toh, S., 2007. Fluidization of granular material in a subduction thrust at seismogenic depths. Earth and Planetary Science Letters 259 (3–4), 307–318.
Unsworth, M.J., Malin, P.E., Egbert, G.D., Booker, J.R., 1997. Internal structure of the San Andreas Fault at Parkfield, California. Geology 25, 359–362.
Vikre, P.G., 1994. Gold mineralization and fault evolution at the Dixie Comstock Mine, Churchill County, Nevada. Economic Geology and the Bulletin of the Society of Economic Geologists 89, 707–719.
Vrolijk, P., van der Pluijm, B.A., 1999. Clay gouge. Journal of Structural Geology 21 (8–9), 1039–1048.
Wallace, R.E., Whitney, R.A., 1984. Late Quaternary History of the Stillwater Seismic Gap, Nevada.
Wibberley, C.A.J., 2002. Hydraulic diffusivity of fault gouge zones and implications for thermal pressurization during seismic slip. Earth. Planets and Space 54 (11), 1153–1171.
Wilden, R., Speed, R.C., 1974. Geology and mineral resources of Churchill County, Nevada. Nevada Bureau of Mines and Geology Bulletin 83, 95.
Woodcock, N.H., Dickson, J.A.D., Tarasewicz, J.P.T., 2007. Transient permeability and reseal hardening in fault zones; evidence from dilation breccia textures. In: Lonergan, L., Jolly, R.J.H., Rawnsley, K., Sanderson, D.J. (Eds.), Fractured reservoirs, 270. Geological Society Special Publications, London, pp. 43–53.